Assessment of Length and Bundle Distribution of Dilute Single-Walled Carbon Nanotubes by Viscosity Measurements

A. Nicholas G. Parra-Vasquez and Juan G. Duque
Dept. of Chemical and Biomolecular Engineering, Rice University, Houston, TX 77005

Richard E. Smalley Institute for Nanoscale Science and Technology, Rice University, Houston, TX 77005

Physical Chemistry and Applied Spectroscopy, Chemistry Division, Los Alamos National Laboratory, Los Alamos, NM 87544

Micah J. Green
Dept. of Chemical and Biomolecular Engineering, Rice University, Houston, TX 77005

Richard E. Smalley Institute for Nanoscale Science and Technology, Rice University, Houston, TX 77005

Dept. of Chemical Engineering, Texas Tech University, Lubbock, TX 79409

Matteo Pasquali
Dept. of Chemical and Biomolecular Engineering, Rice University, Houston, TX 77005

Richard E. Smalley Institute for Nanoscale Science and Technology, Rice University, Houston, TX 77005

Dept. of Chemistry, Rice University, Houston, TX 77005

Dept. of Materials Science and NanoEngineering, Rice University, Houston, TX 77005

DOI 10.1002/aic.14325
Published online January 13, 2014 in Wiley Online Library (wileyonlinelibrary.com)

Rheological measurements have long been an invaluable technique in studying mechanical and structural properties of polymers. Measurements on dilute, noninteracting polymer solutions allow the determination of macromolecular structural information, such as molecular weight. This analysis has been complicated by molecular polydispersity; thus, average effects are more commonly reported. Here, we demonstrate polydispersity characterization for rod-like polymers like single-walled carbon nanotubes (SWCNTs). By extending the theory of the rheological behavior of rigid rods, we determine the distribution of length and bundle size in suspensions of SWCNTs by a simple rheological method. The method is based on measuring the viscosity of dilute suspended SWCNTs over a shear rate range spanning the Newtonian and shear-thinning regimes. We show that a log-normal distribution in length with minimal bundling accurately describes the viscosity measurements. This rapid new method yields the SWCNT length distribution while relying on bulk samples, which are less prone to artifacts. © 2014 American Institute of Chemical Engineers *AIChE J*, 60: 1499–1508, 2014
Keywords: carbon nanotubes, rheology, polydispersity, atomic force microscopy, shear thinning

Introduction

Many key properties of high-performance materials and devices based on single-walled carbon nanotubes (SWCNTs)—and more generally (CNTs)—show a strong dependence on the length and degree of bundling of the constituent SWCNTs. With few exceptions, CNT synthesis methods generate length and diameter-polydisperse CNTs.[1] In addition, typical techniques for dispersing CNTs in liquids produce a mixture of individually dispersed and bundled-CNTs, both of whom typically behave as individual Brownian particles.[2]

Applications strongly influenced by CNT length and bundling are numerous.[3] Both theory and experiment agree that the electrical percolation threshold of CNT-loaded polymer nanocomposites varies inversely with aspect ratio, which is affected by both length and bundle distribution.[3] Similarly, electrical connectivity in CNT thin films, sheets, and buckypapers is affected by length and bundle distribution.[4–11] Mechanical properties of neat CNT fibers scale with length of the constituent CNTs[12]; theoretical predictions on this front were recently experimentally confirmed.[13] Percolation, (including gelation, i.e., rheological percolation) also depends directly on the length of the constituent nanotubes.[14,15] Even biological interactions of SWCNTs are strongly affected by length.[16–19] Finally, in liquid CNT dispersions, the length and bundling

Additional Supporting Information may be found in the online version of this article.

Correspondence concerning this article should be addressed to M. Pasquali at mp@rice.edu.

distribution controls viscoelastic properties,[20–22] gelation, and liquid-crystalline phase transitions.[23]

In our previous work, we demonstrated that this coupling between length and viscosity in the dilute limit can be utilized as a measurement technique.[24] Individually suspended, short (below ~10 μm) SWCNTs behave as rigid rods[25]; thus, their average length can be directly estimated from the zero-shear viscosity of dilute SWCNT suspensions, using theories for the viscosity of dilute suspensions of rods.[26,27]

Various techniques have been used to measure SWCNT length distributions as reviewed recently by Fagan et al.[28] Briefly, the most common technique is atomic force microscopy (AFM) which utilizes a small dispersion sample deposited on a substrate and imaged in tapping mode.[29–32] Despite its commonplace usage, this method is time consuming and relies on relatively small sample size (thousands of CNTs); difficulties with imaging software's ability to distinguish bundles from individuals are also problematic.[24] Similar issues affect other microscopy-based methods.

Bulk techniques are preferred because they are independent of user input and sample separation, and provide rapid throughput. Flow field fractionation utilizes differential entrainment in a parabolic flow field; this method is promising but relies on precise calibration and standards and has not been widely adopted. Dynamic light scattering has also been used to estimate length distribution estimates[33,34]; as noted by Fagan et al.,[28] multiangle scattering measurements must be used to avoid oversimplifying assumptions.

Here, we focus on characterizing the full SWCNT length and bundling distributions. We demonstrate that rheological data on dilute SWCNT dispersions can be used to provide rapid, reliable, objective estimates of the distribution of length and bundle size in the dispersed samples. This work represents a classic example of bulk rheological properties reflecting nanoscale geometry, as modeled by Bird et al.[26]

Theory

Monodisperse rods

The dependence of shear viscosity on shear rate for dilute Brownian rods was determined by Kirkwood (Figure 1a).[35] At low shear rates $\dot{\gamma}$, the viscous torque is lower than the Brownian torque, and the rod orientational distribution is unaffected by the flow; hence, the suspension behaves as a Newtonian liquid, with shear-independent viscosity. As the shear rate grows, a transition regime appears, where the rods start aligning with the flow. At a high enough shear rate, the progressive alignment process yields a terminal shear-thinning regime, where the rod contribution to the viscosity falls with a power law exponent of $-1/2$. In the Kirkwood ansatz, the rod contribution to the viscosity falls all the way to zero because the rods have vanishing cross section; this is a good approximation for rods with high aspect ratio. The zero-shear viscosity η_0 is the limiting value of the ratio of measured shear stress to an imposed vanishingly small shear rate $\dot{\gamma}$. In a solution or suspension, η_0 is the sum of the solvent viscosity η_s and a contribution due to the suspended objects. When such a solution or suspension is dilute, molecules or particles do not interact with each other; therefore, the change in viscosity of such dilute fluids depends linearly on the concentration of the suspended objects.

Following the theoretical development described in our previous publication[24] with a more accurate representation of rod friction in flow,[36] in a dilute suspension of rods the intrinsic viscosity is

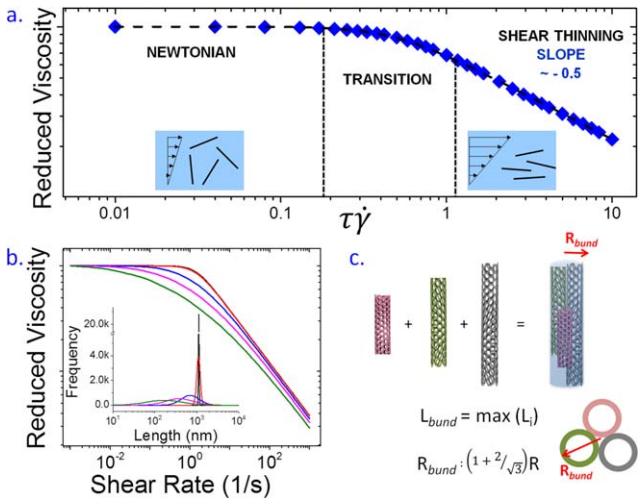

Figure 1. (a) Schematic depicting viscosity-shear rate relationship for dilute Brownian rigid rods; (b) simulated data depicting the effect that length distribution has on the viscosity-shear rate curve; a broader distribution (insert) results in a broader transition from Newtonian to terminal shear thinning; (c) schematic of dominant bundling mechanism and the derived bundle length and radius.

[Color figure can be viewed in the online issue, which is available at wileyonlinelibrary.com.]

$$[\eta] = \lim_{\phi \to 0} \frac{\eta_0 - \eta_s}{\phi \eta_s} = \frac{8}{45}\left(\frac{L}{D}\right)^2 \frac{1}{\ln\left(2L/(R_s \exp\left(25/12\right)\right)} f_M \quad (1)$$

where ϕ is the volume fraction of rods in solution, L and D are the length and diameter of the rod, respectively, and R_s refers to the effective radius of the rod, defined as the point where the fluid adheres to the rod. In a SWCNT-surfactant complex, the effect of the surfactant size a must be considered in estimating the effective radius of the SWCNT-surfactant complex as $R_s = R + a$, where a is the surfactant size. The same analysis applies when any molecule, such as DNA, is used to stabilize individual SWCNTs by wrapping them. For a slender rod in laminar flow, where the fluid adheres to the surface, f_M was determined to be[36–38]

$$f_M = \frac{1 - \frac{0.824}{\ln A_s} + \frac{1.024}{(\ln A_s)^{1.86}} - \frac{0.082}{(\ln A_s)^{4.22}} + \frac{1.331}{(\ln A_s)^{6.36}}}{1 - \frac{0.773}{\ln A_s} + \frac{1.202}{(\ln A_s)^{3.77}} + \frac{0.527}{(\ln A_s)^{3.85}} + \frac{1.088}{(\ln A_s)^{10.65}}} \quad (2)$$

where A_s is the aspect ratio $L/2R_s$ of the rod. In the dilute regime, the viscosity increases linearly with concentration of rods; however, as the rods are noninteracting, the rotational relaxation time τ_{rot} is independent of concentration. Therefore, the reduced viscosity η_{red}, for a given A_s, should overlay for all dilute concentrations.[24] In 1956, Kirkwood and Plock[35] expanded the Kirkwood–Auer relationship to calculate η_{red} as a function of rotational Peclet number, $\tau_{rot}\dot{\gamma}$. (Note that this is equivalent to a Weissenberg number as τ_{rot} is the longest relaxation time in the fluid.) They estimated the reduced viscosity for a slender rod ($A_s > 100$) as

$$\eta_{red}(\dot{\gamma}) = \frac{\eta - \eta_s}{\eta_s \phi} = \frac{8{A_s}^2}{45 \ln 2A_s}\left[1 - 0.729(\tau_{rot}\dot{\gamma})^2 + 1.011(\tau_{rot}\dot{\gamma})^4 \ldots\right] \quad (3)$$

τ_{rot} is defined by the competition between Brownian torques that act so as to randomize rod orientation and viscous

torques resisting relative motion between the rod and the surrounding liquid. This ratio yields a characteristic rotational diffusion time

$$\tau_{\text{rot}}(L,R_s)=\frac{\pi\eta_s L^3}{18k_BT}\left(ln\left(\frac{2L/R_s}{exp(25/12)}\right)\right)^{-1}f_M \quad (4)$$

where k_B is the Boltzmann constant and T is the absolute temperature.[24,36] Eq. 4 has been validated experimentally for surfactant-stabilized SWCNTs suspended in water.[39]

The computational results of Kirkwood and Plock,[35] shown as blue diamonds in Figure 1a, can be fitted to a Carreau–Yasuda equation (shown to fit within 1.3% as dashed line in Figure 1a), resulting in an equation for the viscosity as a function of τ_{rot} and $\dot{\gamma}$

$$\eta=\eta_s+\frac{4}{3}G_0\tau_{\text{rot}}\left[1+(\tau_{\text{rot}}\dot{\gamma}/\theta)^{\alpha}\right]^{(-n/\alpha)} \quad (5)$$

where G_0 is the elastic shear modulus

$$G_0=\frac{3}{5}k_BTv \quad (6)$$

where the number of rods per unit volume v is determined from the volume fraction by dividing by the volume of one rod

$$v=\frac{4\phi}{\pi D^2L} \quad (7)$$

In the case of SWCNTs, ϕ is determined by dividing the mass concentration by the SWCNT density. In the Carreau–Yasuda equation, n, α, and θ are fitting parameters. n controls the slope of the viscosity at high shear rates; thus, $n=1/2$. The parameter α controls the size of the region between the plateau of the zero-shear viscosity and the constant shear-thinning region, best fit by $\alpha=2.405$. The parameter θ controls the shear rate at which shear thinning starts, determined to be $\theta=0.485$.

Polydisperse rods

SWCNT samples are polydisperse both in length and diameter; we assume that SWCNT diameter and length are uncorrelated. The diameter distribution of HiPco SWCNTs[40] ($D=0.98\pm0.21$ nm) and Laser Oven SWCNTs[41] ($D=1.34\pm0.30$ nm) are so narrow that treating the sample as monodisperse in diameter introduces minimal error (e.g., $\langle D^2\rangle$ and $\langle D\rangle^2$ differ by 5%). However, like other polymers, SWCNTs display significant length polydispersity.[1]

Given a continuous length distribution, the distribution function is defined as $\Omega(L)$. From the length distribution, the jth moment of L is defined as

$$\langle L^j\rangle=\int_0^{\infty}L^j\Omega(L)dL \quad (8)$$

The first moment of L is known as the mean length μ_L and the standard deviation σ_L of L is defined as

$$\sigma_L\equiv\sqrt{\langle L^2\rangle-\langle L^2\rangle}=\sqrt{\frac{N}{N-1}\frac{1}{N}\left(\sum_{i=1}^{N}L_i^2-\left(\frac{1}{N}\sum_{i=1}^{N}L_i\right)^2\right)} \quad (9)$$

where the second representation is for a discrete population of N members, that is, a length distribution produced with AFM.

Because dilute rods are noninteracting, polydispersity can be incorporated into Eq. 5 by integrating over the entire length distribution

$$\eta=\eta_s+\frac{4}{5}k_BTv\int_0^{\infty}\tau_{\text{rot}}(L,R_s)\left[1+\left(\frac{\tau_{\text{rot}}(L,R_s)\dot{\gamma}}{\theta}\right)^{\alpha}\right]^{(-n/\alpha)}\Omega(L)dL \quad (10)$$

where the number density v is determined from the average volume of the rods

$$v=\frac{4\phi}{\pi D^2\mu_L} \quad (11)$$

and $\tau_{\text{rot}}(L,R_s)$ is given in Eq. 4.

A more physical understanding of the effect of polydispersity is illustrated in Figure 1b. Five distributions of length varying in degree of polydispersity, but chosen with the same zero-shear viscosity, were used to simulate viscosity data over a range of shear rates. Narrowly peaked distributions result in a sharp transition from Newtonian at low shear rates to terminal shear thinning at higher shear rates. As the polydispersity increases, longer rods begin to align and shear thin at lower shear rates and shorter rods achieve terminal shear thinning at higher shear rates, thus, broadening the region between the two. Therefore, to capture the full distribution, it is important to measure the viscosity in a range of shear rates between the Newtonian and terminal shear-thinning regions.

Bundling of nanotubes

Recent experimental results have raised questions on the degree of bundling in SWCNT suspensions. O'Connell et al.[42] estimated that sonicating SWCNTs in water in the presence of surfactants, followed by ultracentrifugation, yields suspensions where 90% of the SWCNTs are individuals; later studies estimated this procedure yields fewer individualized SWCNTs, typically 50% (based on samples that have gone through a density-gradient ultracentrifugation).[43–45] Cathcart et al.[43] estimate that dilute SWCNTs stabilized by DNA wrapping have as few as 83% individual SWCNTs. However, as bundles of SWCNTs are effectively rod-like, dispersed Brownian objects, the theory can accommodate the presence of bundles.

The rotational relaxation time $\tau_{\text{rot}}(L,R_s)$ depends only on the geometry of the rod. Thus, bundling affects τ_{rot} because the geometry, dictated by L_{bund} and R_{bund}, will change. The suspension preparation procedure yields two observations. First, the suspended bundles are small, as they remain in the supernatant after ultracentrifugation. Second, these suspended small bundles were not broken apart during sonication, indicating that they are closely held together by van der Waals forces, which are maximized when the sidewalls of the SWCNTs within the bundle contact each other completely. Thus, we estimate bundle size by assuming that shorter SWCNTs within a bundle are in full contact with the longest SWCNT, that is, the bundle length is that of its longest constituent SWCNT. The bundle radius depends on the number of SWCNTs within the bundle, as depicted in Figure 1c.

The probability that any individual SWCNT has a length X below L' is

$$P\left(X\le L'\right)=\int_0^{L'}\Omega(L)dL \quad (12)$$

Given a bundle of k SWCNTs, then the probability of this bundle having a length below L' is the same as the

probability of each SWCNT within the bundle independently having a length below L'. This probability is

$$P\left(X_i < L' | N=k\right) = P\left(X_1 \le L'\right)P\left(X_2 \le L'\right)\ldots$$
$$P\left(X_k \le L'\right) = \left(\int_0^{L'} \Omega(L)dL\right)^k \quad (13)$$

A bundle probability distribution is needed to progress further. Such distribution should reflect the assumptions made on bundles that survive sample preparation. Ultracentrifugation drives larger bundles out of solution; thus, the smaller bundles have a higher probability of remaining in solution than larger ones. An exponentially decaying function is a simple and convenient distribution that meets these criteria. (We have also tried a linear decay probability resulting in minimal fitting error <1%; see Supporting Information Figure S1.) Therefore, we assume that the probability of finding a bundle of k SWCNTs is independent of length and follows an exponential decay

$$P(N=k) = \frac{\exp(-\xi k)}{\sum_{j=1}^{N_{\max}} \exp(-\xi j)} \quad (14)$$

where $N_{\max}$ is the maximum bundle size allowable and ξ is a parameter that defines how sharply the probability of finding a bundle of k rods decreases as k increases; ξ is sample dependent and is used as a fitting parameter. (e.g., a sample contains 50% individuals when $\xi = 0.693$.)

Finally, as Eq. 14 is independent of length, the probability of finding a bundle of k rods and length below L' is

$$P\left(N=k, X_i \le L', i=1,2,\ldots k\right)$$
$$= P(N=k)P\left(X_i \le L' | N=k\right)$$
$$= \left(\int_0^{L'} \Omega(L)dL\right)^k \frac{\exp(-\xi k)}{\sum_{j=1}^{N_{\max}} \exp(-\xi j)} \quad (15)$$

For a given length distribution of SWCNT length, bundling shifts the average rod length to higher lengths and also reduces the number density of suspended "rods" v. By a similar analysis, v can be determined from the volume fraction by dividing the average volume of the suspended bundles

$$v = \frac{\phi}{V_{\text{bund}}} \quad (16)$$

where V_{bund} is calculated similarly to Eq. 8 using both length and bundle probability distributions

$$V_{\text{bund}} = \sum_{k=1}^{N_{\max}} \left[\int_o^{\infty} \pi L R_{\text{bund}}^2(k) k \left(\int_0^L \Omega(t)dt\right)^{k-1} \Omega(L)dL\right] \frac{\exp(-\xi k)}{\sum_{j=1}^{N_{\max}} \exp(-\xi j)} \quad (17)$$

The bundling is then incorporated into Eq. 10 by summing over the bundle distribution

$$\eta = \eta_s + \frac{4}{5} k_B T v \sum_{k=1}^{N_{\max}} \left[\int_o^{\infty} \tau_{\text{rot}}^* \left[1 + \left(\frac{\tau_{\text{rot}}^* \dot{\gamma}}{\theta}\right)^{\alpha}\right]^{(-n/\alpha)} k \left(\int_0^L \Omega(t)dt\right)^{k-1} \Omega(L)dL\right] \frac{\exp(-\xi k)}{\sum_{j=1}^{N_{\max}} \exp(-\xi j)} \quad (18)$$

where v is calculated using Eq. 16 and $\tau_{\text{rot}}^* = \tau_{\text{rot}}(L, R_{\text{bund}}(k)+a)$, defined in Eq. 4. Note that if all SWCNTs are individuals, $N_{\max}$ is 1 and ξ is infinite; in that case Eq. 18 reduces to Eq. 10, and Eq. 16 reduces to Eq. 11.

This study uses a log-normal distribution, previously found to closely represent AFM distributions of produced SWCNTs.[24,46,47] The log-normal distribution is defined by two parameters, the average μ and standard deviation σ of $\ln(L)$. The probability distribution function is then written as

$$\Omega(L) = \frac{1}{L\sigma\sqrt{2\pi}} \exp\left(-\frac{(\ln L - \mu)^2}{2\sigma^2}\right) \quad (19)$$

Parameter determination procedure

A sample of suspended SWCNTs is described by three parameters: μ and σ of the log-normal distribution and ξ of the bundle distribution. The rheological data yields a set of viscosity measurements at p shear rates (typically $p \approx 20$) and q concentrations (typically $q \approx 2$–4), for a total of pq data points. Equation 18 yields a relationship between the three unknown parameters for each shear rate, resulting in an overspecified system of pq equations in three unknowns, which are determined with a Levenberg–Marquardt parameter estimation algorithm (schematically depicted in Figure 2).

We found that the fitted values of μ, σ, and ξ depend on the error metric used. An absolute error metric places disproportionate weight on data measured at low shear rates because the viscosity values are higher at low shear rates. To remedy this, we used a relative error ε, the absolute difference between measured and calculated torque relative to the instrument sensitivity

$$\varepsilon = \frac{M - \overline{M}}{M_{\text{inst}}} \quad (20)$$

where M is the measured torque, $\overline{M}$ is the calculated torque for the distribution being fit, and M_{inst} is the instrument sensitivity, shown in Supporting Information Figure S2. The use of ε gives a strong solution of minimal error, as shown in an error contour plot, Supporting Information Figure S3. Notably, any additional knowledge of the distribution, such as AFM data, can be used to help determine the best fit parameters (Supporting Information Figure S4).

Experimental Procedures

DNA dispersions of HiPco SWCNTs

Single-stranded (ss) DNA [30-mer oligonucleotide, sequence (GT)15, from Integrated DNA Technologies] was used to disperse SWCNT in water. Aqueous dispersions of SWCNTs were achieved by sonication (0.32-cm tip sonicator, Thomas Scientific) of HiPco SWCNTs (Carbon Nanotechnologies, HiPco Batch 286) in salt solution (200 mmol/L NaCl, 40 mmol/L Tris, 0.2 mmol/L NaN3 buffered to pH 7 with HCl) followed by ultracentrifugation at 21,000 g for 2 h to remove large bundles. SWCNT and DNA were at concentrations of

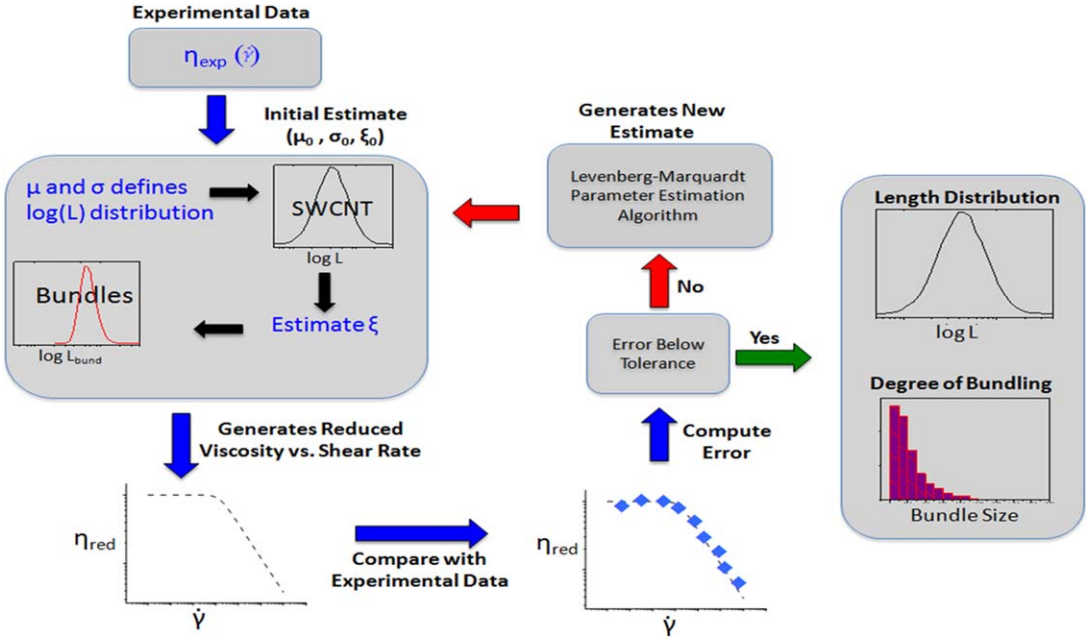

Figure 2. Schematic describing the model parameter fitting process based on bulk rheological measurements.

First, the viscosity data are supplied to the program, along with an initial estimate for the three parameters. The viscosity is calculated as a function of shear rate and compared with the data. The error is then computed and if it is within a set tolerance, then the length and bundle distributions have been determined. If the tolerance is not met, a Levenberg–Marquardt parameter estimation algorithm is used to compute new parameter estimates. The cycle is repeated until the tolerance has been met and the distributions determined. [Color figure can be viewed in the online issue, which is available at wileyonlinelibrary.com.]

1 mg/mL.[48] By combining the average carbon-carbon diameter of HiPco material, 0.93 nm,[49] to twice the van der Waals radius of carbon, 0.17 nm, we estimate that the average external diameter of the SWCNTs in our sample is $D = 1.27$ nm.

To increase the viscosity of the solution, a 50 wt % sugar mixture (60/40 sucrose/glucose) was added to both the SWCNT dispersions and the salt solution. The solvent viscosity increased from 1 to 12 mPa s and remained Newtonian, indicating no structure formation. The increase in viscosity had two positive effects: the viscosity could be measured accurately at lower shear rates (more accurate zero-shear viscosity) and the onset of shear thinning (important for determining length distribution) shifted to lower shear rates, within the range of the instrument. DNA does not uniformly wrap around the SWCNT; however, it disperses SWCNTs as individuals. The ssDNA protrudes from the surface of the SWCNT about 1.0 ± 0.5 nm.[50,51] Fluorescence measurements were taken before and after addition of sugar and showed no changes in intensity, that is, the local environment of the SWCNTs was unchanged. Moreover, Raman measurements at 785 nm show no changes in the "bundling peak" (260 cm^{-1}) after addition of sugar (Supporting Information Figure S5). From these, we conclude that the sugar causes insignificant bundling[52–54]; thus, the distribution is not altered.

Deoxycholate dispersions of laser ablation SWCNTs

Surfactant-stabilized laser ablation SWCNT dispersions (NASA-JSC soot #338) were prepared by a sonication, centrifugation, and decant process.[55] The average diameter of these SWCNTs is 1.34 nm[41]; combining with van der Waals radius of carbon yields an average external diameter of $D = 1.69$ nm. A 1 wt % solution of sodium deoxycholate (DOC, from Sigma Aldrich), a small surfactant with a molecular weight of 414.55 g/mol, was used to suspend SWCNTs in water. DOC is known to form cylindrical micelles; the SWCNTs occupy the center of the micelle. The DOC molecule protrude from the surface of the SWCNTs giving a radius enhancement of 1.0 ± 0.2 nm.[56]

Absorbance

The concentrations of the aqueous dispersions were estimated by Ultraviolet-Vis spectroscopy using the extinction coefficient 0.043 L/(mg cm) at 763 nm.[57] The concentrations were converted to volume fraction, which was used to calculate rod number density in Eq. 16, by using a SWCNT density of 1.45 g/cm^3 for HiPco nanotubes [close-packed density for (7,8) SWCNTs] and 1.24 g/cm^3 for Laser Ablation nanotubes [close-packed density for (10,10) SWCNTs].

Rheology

Low concentrations were tested to ensure that measurements were in the dilute regime; this occurs in suspensions whose viscosity is roughly below twice the solvent viscosity.[27] The dispersion with the highest concentration was diluted to make several different concentrations. Dispersions at low concentrations with viscosities within 5% of the solvent were not used because of the large subtraction error when calculating the reduced viscosity, η_{red}. Each diluted sample was tested on an ARES strain-controlled rheometer (Rheometrics Scientific, now TA Instruments) at shear rates $\dot{\gamma}$ from 0.01 to 100 s^{-1} in a Couette fixture, either a titanium bob and 316 stainless steel cup, (height 34 mm, cup diameter 34 mm, bob diameter 32 mm, 1 mm gap, torque sensitivity ~0.1 μN m, corresponding to a minimum measurable shear stress of 1.83 mPa) or a double-walled Couette fixture (height 30 mm, bob: $R1 = 14.75$ mm, $R2 = 16$ mm, cup: $R1 = 13.975$ mm, $R2 = 17.00$ mm, 1 mm outer gap and 0.775 mm inner gap, minimum measurable shear stress of

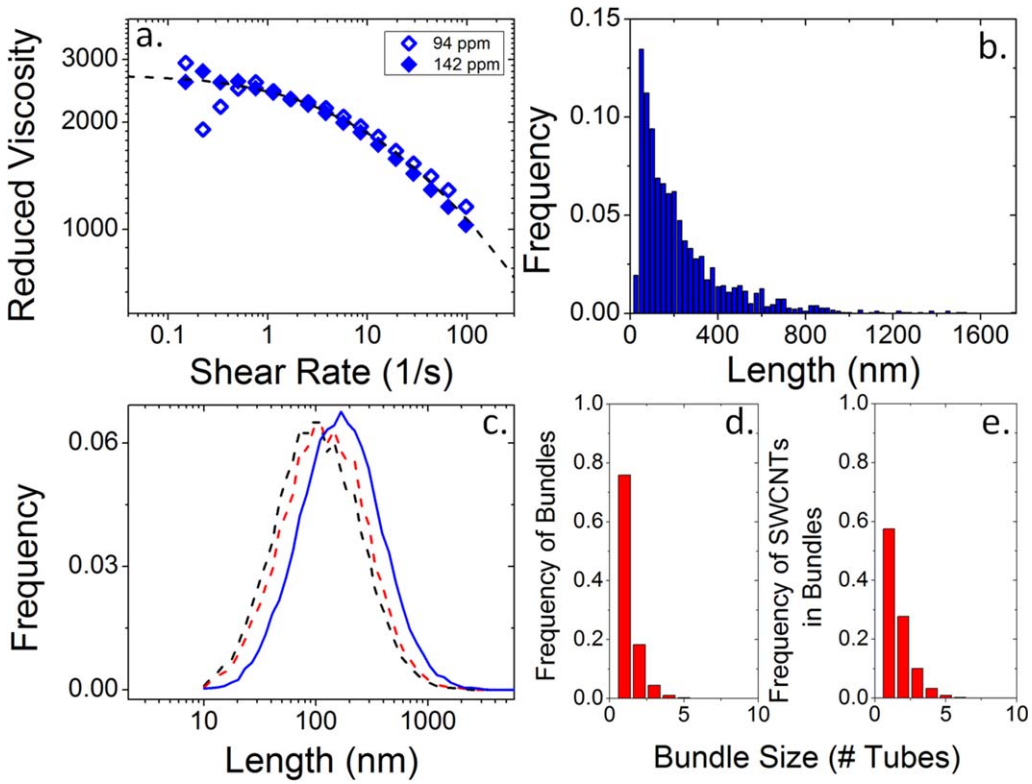

Figure 3. (a) Reduced viscosity vs. shear rate for SWCNTs dispersed using DNA at two concentrations (blue) and the calculated reduced viscosity for the best fit distribution (black).

(b) AFM distribution of DNA-dispersed SWCNTs. 1753 individual SWCNTs measured. (c) Comparison of AFM log-normal distribution (blue), viscosity fit distribution (black), and shifted viscosity fit distribution due to bundling (red). Distributions of bundle sizes in the DNA/SWCNT dispersion show that, (d) 76% of the Brownian objects are individuals, and (e) 58% of all nanotubes in solution exist as individuals. [Color figure can be viewed in the online issue, which is available at wileyonlinelibrary.com.]

1.12 mPa). A vapor trap was used to maintain a moisture-saturated environment preventing solvent evaporation.

AFM

AFM (NanoScope R IIIa, Veeco Instruments) samples of SWCNT dispersions in aqueous DOC and DNA solutions were prepared by spin coating at 3000 rpm onto a freshly cleaved mica surface (Ted Pella), followed by rinsing with deionized (DI) water and isopropanol to remove the excess surfactant or sugar. All AFM images were taken in tapping mode at a scan rate of 1.25 Hz and scan sizes of 5 and 10 μm.

Results and Discussion

In the dilute regime, the reduced viscosity η_{red} of dilute suspensions overlays at all shear rates.[24] Thus, the data measured at all concentrations can be used in the fitting procedure. The length and bundle distribution for two test systems with varying SWCNT source and surfactant is determined by viscosity measurements and then compared with AFM distributions. The utility of this method confirms the general applicability of the theoretical formulation described above.

A careful analysis of the difference between AFM and viscosity-based methods in regard to repeatability, sensitivity, and efficiency is described in our prior publication.[24] Also, note that all methods above to disperse SWCNTs require ultrasonication to debundle and disperse the SWCNTs; this technique is known to shorten SWCNTs as well.[28,58,59]

Case 1: DNA dispersions of HiPco SWCNTs

We studied DNA-stabilized HiPco SWCNTs suspended in water and sugar (used to raise the solution viscosity and lower the critical shear rate for shear thinning). The measured reduced viscosity of these suspensions overlay for both concentrations at all shear rates (Figure 3a, blue). The zero-shear reduced viscosity is 2510 ± 380, which results in a viscosity average length of 288 ± 17 nm.[24] A log-normal distribution with $\mu = -16.1$ (102 nm) and $\sigma = 0.866$ accurately fits the data (Figure 3c, black). For comparison, the distribution of Brownian objects, both individual SWCNTs and small bundles, is shown in red. The bundling of SWCNTs shifts the mean to longer length and slightly decreases the standard deviation; this is expected because each bundle acts as an entity with a length equal to that of its longest SWCNT.

The DNA-stabilized suspensions were found to contain a small amount of bundles. Figure 3d shows that 76% of the Brownian objects were individual SWCNTs; the remaining 24% were bundles of five SWCNTs or less. In comparing with the total amount of SWCNTs, Figure 3e shows that 58% of all the SWCNTs in solution were individualized; these values fall in the range found by Cathcart et al.[43]

For AFM characterization, the sample was rinsed while spin coating, first with warm water to dissolve the sugar and then with isopropanol to dry the sample. AFM revealed that most SWCNTs were individualized; 1753 individual SWCNTs were measured, shown in Figure 3b, giving a log-normal distribution with a μ and σ of −15.63 (163 nm) and 0.845, respectively (Figure 3c, red).

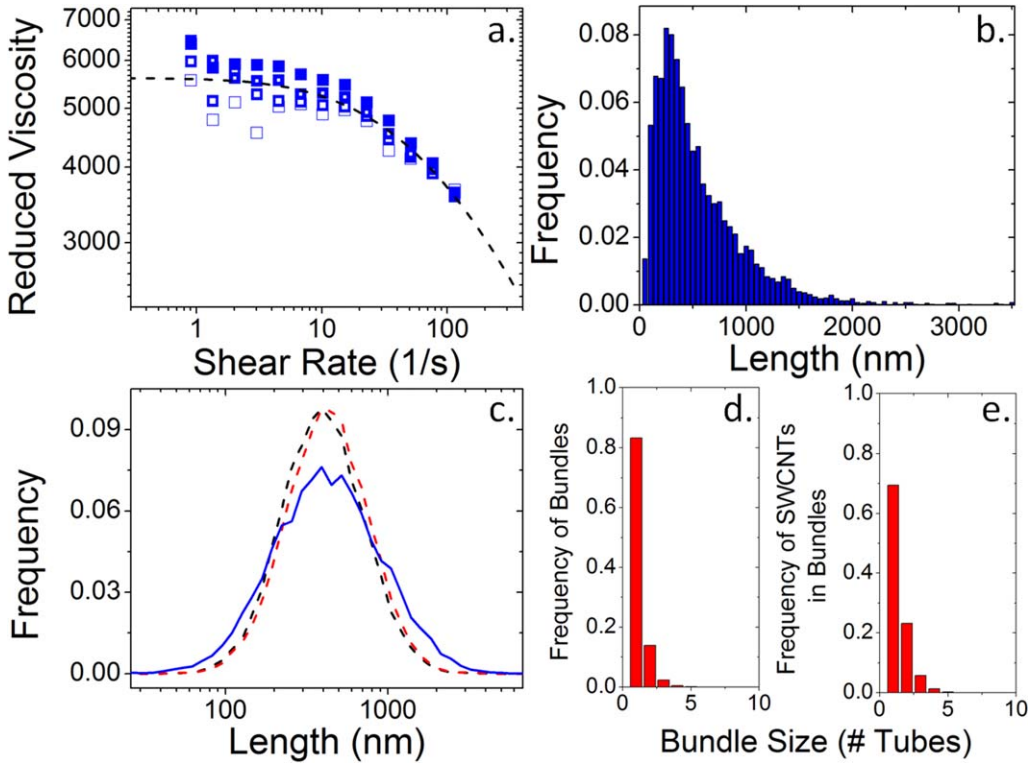

Figure 4. (a) Reduced viscosity vs. shear rate for SWCNTs dispersed using DOC at four overlaying concentrations (37, 46, 67, and 97 ppm, in blue) and the calculated reduced viscosity for the best fit distribution (black).

(b) AFM distribution of DNA-dispersed SWCNTs. 3793 individual SWCNTs measured. (c) Comparison of AFM log-normal distribution (blue), viscosity fit distribution (black), and shifted viscosity fit distribution due to bundling (red). Distributions of bundle sizes in the DOC/SWCNT dispersion reveal more individual SWCNTs than in DNA/SWCNT dispersion. (d) 84% of the Brownian objects are individuals, and (e) 70% of all nanotubes in solution exist as individuals. [Color figure can be viewed in the online issue, which is available at wileyonlinelibrary.com.]

The distributions found by viscosity measurements and by AFM are very similar. The average length differs by 60%, 102 nm vs. 163 nm, whereas the standard deviation σ or distribution spread are nearly the same, 0.867 and 0.845 for viscosity and AFM distributions, respectively. This small difference is shown in Figure 3c; both distributions have the same shape or width, defined by σ, but the AFM distribution (blue) is shifted to the right because of the greater μ value. Included for comparison is the distribution of Brownian objects (individuals and bundles, shown in red), which define the fit viscosity. As expected, the presence of bundles causes the value of μ to shift right toward higher lengths and closer to the AFM distribution.

A common method to show the quality of a distribution fit to data is a probability-probability (p-p) plot (Supporting Information Figure S6). The p-p plot confirms that a log-normal distribution fits the AFM measured data well, except at low values of the cumulative distribution function (short lengths), where the AFM fit predicts shorter SWCNTs than were measured.

This is caused by AFM's difficulty in distinguishing small nanotubes (<30 nm) from particles adhered to the surface when measuring 5–10 μm scans. Scanning smaller areas will improve the resolution, enabling distinction of small nanotubes but will cut off longer nanotubes. The viscosity distribution is able to measure all contributing lengths and, thus, able to capture the smaller nanotubes resulting in a lower average length.

Case 2: DOC dispersions of laser ablation SWCNTs

A laser ablation-produced SWCNT sample dispersed in water using sodium DOC was also studied because this sample displayed a higher average length than HiPco SWCNTs. (Short SWCNTs are more likely to skew AFM distribution measurements as noted above.)

Without addition of sugar, the viscosity measurements showed shear thinning within the measurable shear rate range of the instrument, suggesting longer SWCNTs than in the DNA-stabilized suspensions of HiPco SWCNTs. The reduced viscosity measurements of the DOC/laser ablation SWCNT dispersions overlay for all concentrations at all shear rates (Figure 4a, blue). The zero-shear viscosity is measured as 5570 $\pm$ 835; accounting for the larger diameter of the laser ablation SWCNTs ($\sim$1.34 nm) results in an average length of 616 $\pm$ 31 nm. A log-normal distribution with a μ of -14.74 (397 nm) and a σ of 0.574 accurately fits the data, shown in Figure 4a, black.

The DOC/laser ablation SWCNT system includes a larger proportion of individually dispersed SWCNTs than the DNA/HiPco SWCNT system. Figure 4d shows that 84% of all objects in solution are individual SWCNTs, and Figure 4e shows that 70% of all nanotubes in solution are individuals.

AFM was also used to characterize this system. A total of 3793 individual SWCNTs were measured to obtain the length distribution shown in Figure 4b. The longer SWCNTs give a more developed distribution on the left side of the

maximum than Figure 3b, which results in a better log-normal distribution fit (Supporting Information Figure S6). The μ and σ of the log-normal distribution that fit the AFM data are -14.69 (419 nm) and 0.758, respectively, shown in Figure 4c, blue.

The μ of the viscosity fit (black) and AFM fit distribution (blue) are nearly identical and the small amount of bundling shows only a small shift in the fit distribution (red), shown in Figure 4c. There is a difference in the σ values (0.577 vs. 0.758); the AFM data show a broader distribution. (AFM is merely a snapshot of the distribution viewing $\sim$4000 nanotubes rather than $\sim 10^{15}$ nanotubes measured by viscosity.[24]) The p-p plot (Supporting Information Figure S6) confirms the AFM fit distribution and viscosity fit distribution both closely fit the data.

The close fit between distributions from AFM and viscosity data indicate the general applicability of the theory for rigid rods to these systems. Limitations of the theory that may require further refinement mainly concern the treatment of bundles. Each bundle is assumed to act as a rod with a radius estimated from the number of SWCNTs in the bundle and a length equal to that of the longest SWCNT within the bundle. Limitations of this approach include the following: (1) Bundles are not actually cylindrical; the radius of the bundle varies, yielding a rougher surface and higher drag [inversely proportional to $\log(R)$] than the idealized cylinder. The inaccuracy of this assumption is most severe for small (few SWCNT) bundles. However, compared to the drag along the length of the nanotube (proportional to L^3) this enhancement is small.[24] (2) Bundle distributions may differ from Eq. 14, particularly in the assumption that bundling probability is independent of length. (3) It is possible that SWCNTs may bundle such that the length of the bundle is greater than the length of the longest SWCNT in the bundle.[60] These types of bundles will contribute greater viscosity than the type considered above. For distribution fitting, a slightly shorter length distribution with a smaller bundle size distribution is needed to achieve the same reduced viscosity with these types of bundles. However, due to the small amount of bundling, our calculations suggest that these effects yield minor changes in μ and σ. Further empirical data of typical bundle structures will improve the accuracy of the distributions determined by the technique described here. All these limitations are expected to make quantitative rather than qualitative alterations to the expected shear-thinning behavior and data analysis.

Note that to achieve an accurate distribution fit, the full range of viscosity behavior, from Newtonian to shear thinning, is necessary. For example, if the torque at low shear rates is too low, the accuracy of the zero-shear viscosity measurement can be compromised, and a less accurate distribution will be determined as well. We conducted a study using Pluronic F-68 where this was the case (Supporting Information Figures S7–S10).

Conclusions

Using an extension of kinetic theory for rigid rods,[35] we have developed a technique for using bulk viscosity-shear rate measurements as a means to extract polydispersity data for aqueous SWCNT dispersions. We tested this procedure on both SWCNTs dispersed in DNA/sugar and DOC aqueous solutions. The fit SWCNT length distributions were very similar to AFM measurements, except at shorter lengths where AFM was unable to capture the smaller nanotubes present in solution. We also obtained an estimate of the distribution of bundle size by assuming that each small bundle behaves as a Brownian rod as long as it is the longest constituent SWCNT.

This work allows for the theoretical kinetic theory framework developed by Kirkwood and Plock[35] (and later elucidated by Bird et al.[26] and Doi and Edwards[27]) to be applied directly to the rheological behavior of a "model rigid rod" system of dispersed SWCNTs, which have been used in similar studies to elucidate competing models of rigid-rod polymer dynamics.[61] This technique can be easily adapted to other rigid-rod systems and the formulation can accommodate a variety of distributions in length and bundle size. This technique will be particularly useful as novel exfoliation and dispersion methods are developed to allow for scalable liquid-phase SWCNT processing; rapid characterization of dispersion quality, bundle distribution, and exfoliation effects on SWCNT length would facilitate such critical steps in nanomanufacturing.[2]

Acknowledgments

We acknowledge J.A. Fagan at NIST, Gaithersburg, MD, for providing nanotube samples for measurement. We wish to acknowledge funding from AFOSR Grants FA9550-06-1-0207 and FA9550-09-1-0590, the Robert A. Welch Foundation Grant C-1668, and the Evans-Attwell Welch Postdoctoral Fellowship. We thank Stephen Doorn of LANL for access to Raman instrumentation.

Notation

ϕ = rod/SWCNT volume fraction
R_s = effective rod radius
L = rod length
D = rod diameter
a = surfactant/DNA wrapping size
A_s = aspect ratio
V_{bund} = bundle volume
ν = rod number density
η = viscosity
η_s = solvent viscosity
η_{red} = reduced viscosity
$\dot{\gamma}$ = shear rate
τ_{rot} = rotational rod relaxation time
G_0 = elastic shear modulus
n, α, θ = Carreau-Yasuda fitting parameters
$P(X \leq L')$ = probability that a given SWCNT has a length X below L'
$\Omega(L)$ = length probability distribution function
N_{max} = largest bundle size in distribution
μ_L = average of L
σ_L = standard deviation of L
μ = average of ln (L)
σ = standard deviation of ln (L)
ξ = bundle distribution fitting parameter
ε = relative error between measured and calculated torque
M = measured torque
$\overline{M}$ = calculated torque
M_{inst} = instrument torque sensitivity

Literature Cited

1. Green MJ, Behabtu N, Pasquali M, Adams WW. Nanotubes as polymers. *Polymer*. 2009;50:4979–4997.
2. Green MJ. Analysis and measurement of carbon nanotube dispersions: nanodispersion versus macrodispersion. *Polym Int*. 2010;59:1319–1322.
3. Grady BP. *Carbon Nanotube—Polymer Composites*. Hoboken, NJ: Wiley, 2011.

4. Duggal R, Hussain F, Pasquali M. Self-assembly of single-walled carbon nanotubes into a sheet by drop drying. *Adv Mater*. 2006;18: 29–34.
5. Meitl MA, Zhou YX, Gaur A, Jeon S, Usrey ML, Strano MS, Rogers JA. Solution casting and transfer printing single-walled carbon nanotube films. *Nano Lett*. 2004;4:1643–1647.
6. Trottier CM, Glatkowski P, Wallis P, Luo J. Properties and characterization of carbon-nanotube-based transparent conductive coating. *J Soc Inf Disp*. 2005;13:759–763.
7. Wu ZC, Chen ZH, Du X, Logan JM, Sippel J, Nikolou M, Kamaras K, Reynolds JR, Tanner DB, Hebard AF, Rinzler AG. Transparent, conductive carbon nanotube films. *Science*. 2004;305:1273–1276.
8. Zhang XF, Sreekumar TV, Liu T, Kumar S. Properties and structure of nitric acid oxidized single wall carbon nanotube films. *J Phys Chem B*. 2004;108:16435–16440.
9. Hecht D, Hu L, Gruner G. Conductivity scaling with bundle length and diameter in single walled carbon nanotube networks. *Appl Phys Lett*. 2006;89:133112–133113.
10. Dan B, Irvin GC, Pasquali M. Continuous and scalable fabrication of transparent conducting carbon nanotube films. *ACS Nano*. 2009;3: 835–843.
11. Mirri F, Ma AWK, Hsu TT, Behabtu N, Eichmann SL, Young CC, Tsentalovich DE, Pasquali M. High-performance carbon nanotube transparent conductive films by scalable dip coating. *ACS Nano*. 2012;6:9737–9744.
12. Behabtu N, Green MJ, Pasquali M. Carbon nanotube-based neat fibers. *Nano Today*. 2008;3:24–34.
13. Behabtu N, Young CC, Tsentalovich DE, Kleinerman O, Wang X, Ma AWK, Bengio EA, ter Waarbeek RF, de Jong JJ, Hoogerwerf RE, Fairchild SB, Ferguson JB, Maruyama B, Kono J, Talmon Y, Cohen Y, Otto MJ, Pasquali M. Strong, light, multifunctional fibers of carbon nanotubes with ultrahigh conductivity. *Science*. 2013;339:182–186.
14. Bryning MB, Milkie DE, Islam MF, Hough LA, Kikkawa JM, Yodh AG. Carbon nanotube aerogels. *Adv Mater*. 2007;19:661–664.
15. Vigolo B, Coulon C, Maugey M, Zakri C, Poulin P. An experimental approach to the percolation of sticky nanotubes. *Science*. 2005; 309:920–923.
16. Cherukuri P, Bachilo SM, Litovsky SH, Weisman RB. Near-infrared fluorescence microscopy of single-walled carbon nanotubes in phagocytic cells. *J Am Chem Soc*. 2004;126:15638–15639.
17. Fiorito S, Serafino A, Andreola F, Bernier P. Effects of fullerenes and single-wall carbon nanotubes on murine and human macrophages. *Carbon*. 2006;44:1100–1105.
18. Nimmagadda A, Thurston K, Nollert MU, McFetridge PSF. Chemical modification of SWNT alters in vitro cell-SWNT interactions. *J Biomed Mater Res A*. 2006;76A:614–625.
19. Sayes CM, Liang F, Hudson JL, Mendez J, Guo WH, Beach JM, Moore VC, Doyle CD, West JL, Billups WE, Ausman KD, Colvin VL. Functionalization density dependence of single-walled carbon nanotubes cytotoxicity in vitro. *Toxicol Lett*. 2006;161:135–142.
20. Fry D, Langhorst B, Kim H, Grulke E, Wang H, Hobbie EK. Anisotropy of sheared carbon-nanotube suspensions. *Phys Rev Lett*. 2005;95:038304.
21. Fry D, Langhorst B, Wang H, Becker ML, Bauer BJ, Grulke EA, Hobbie EK. Rheo-optical studies of carbon nanotube suspensions. *J Chem Phys*. 2006;124:054703.
22. Hough LA, Islam MF, Janmey PA, Yodh AG. Viscoelasticity of single wall carbon nanotube suspensions. *Phys Rev Lett*. 2004;93: 168102-1-168102-4.
23. Green MJ, Parra-Vasquez ANG, Behabtu N, Pasquali M. Modeling the phase behavior of polydisperse rigid rods with attractive interactions with applications to single-walled carbon nanotubes in superacids. *J Chem Phys*. 2009;131:084901.
24. Parra-Vasquez ANG, Stepanek I, Davis VA, Moore VC, Haroz EH, Shaver J, Hauge RH, Smalley RE, Pasquali M. Simple length determination of single-walled carbon nanotubes by viscosity measurements in dilute suspensions. *Macromolecules*. 2007;40:4043–4047.
25. Fakhri N, Tsyboulski DA, Cognet L, Weisman RB, Pasquali M. Diameter-dependent bending dynamics of single-walled carbon nanotubes in liquids. *Proc Natl Acad Sci USA*. 2009;106:14219–14223.
26. Bird RB, Curtiss CF, Armstrong RC, Hassager O. *Dynamics of Polymeric Liquids, Kinetic Theory*. Wiley, USA: Amazon, google books, 1987.
27. Doi M, Edwards SF. *The Theory of Polymer Dynamics*. New York: Oxford University Press, 1988.
28. Fagan JA, Bauer BJ, Hobbie EK, Becker ML, Hight Walker AR, Simpson JR, Chun J, Obrzut J, Bajpai V, Phelan FR, Simien D, Huh JY, Migler KB. Carbon nanotubes: measuring dispersion and length. *Adv Mater*. 2011;23:338–348.
29. Islam MF, Rojas E, Bergey DM, Johnson AT, Yodh AG. High weight fraction surfactant solubilization of single-wall carbon nanotubes in water. *Nano Lett*. 2003;3:269–273.
30. Wang SR, Liang ZY, Wang B, Zhang C. Statistical characterization of single-wall carbon nanotube length distribution. *Nanotechnology*. 2006;17:634–639.
31. Ziegler KJ, Gu ZN, Shaver J, Chen ZY, Flor EL, Schmidt DJ, Chan C, Hauge RH, Smalley RE. Cutting single-walled carbon nanotubes. *Nanotechnology*. 2005;16:S539–S544.
32. Zaric S, Ostojic GN, Kono J, Shaver J, Moore VC, Hauge RH, Smalley RE, Wei X. Estimation of magnetic susceptibility anisotropy of carbon nanotubes using magnetophotoluminescence. *Nano Lett*. 2004;4:2219–2221.
33. Badaire S, Poulin P, Maugey M, Zakri C. In situ measurements of nanotube dimensions in suspensions by depolarized dynamic light scattering. *Langmuir*. 2004;20:10367–10370.
34. Lee JY, Kim JS, An KH, Lee K, Kim DY, Bae DJ, Lee YH. Electrophoretic and dynamic light scattering in evaluating dispersion and size distribution of single-walled carbon nanotubes. *J Nanosci Nanotechnol*. 2005;5:1045–1049.
35. Kirkwood JG, Plock RJ. The visco-elastic properties of solutions of rod-like macromolecules. *J Chem Phys*. 1956;19:281–283.
36. Mansfield ML, Douglas JF. Transport properties of rodlike particles. *Macromolecules*. 2008;41:5422–5432.
37. Batchelor GK. The stress system in a suspension of force-free particles. *J Fluid Mech*. 1970;41:545–570.
38. Larson RG. The Structure and Rheology of Complex Fluids. New York: Oxford University Press, 1999.
39. Duggal R, Pasquali M. Dynamics of individual single-walled carbon nanotubes in water by real-time visualization. *Phys Rev Lett*. 2006; 96:246104.
40. Kukovecz A, Kramberger C, Georgakilas V, Prato M, Kuzmany H. A detailed Raman study on thin single-wall carbon nanotubes prepared by the HiPCO process. *Eur Phys J B*. 2002;28:223–230.
41. Kingston CT, Simard B. Recent advances in laser synthesis of single-walled carbon nanotubes. *J Nanosci Nanotechnol*. 2006;6; 1225–1232.
42. O'Connell MJ, Bachilo SM, Huffman CB, Moore VC, Strano MS, Haroz EH, Rialon KL, Boul PJ, Noon WH, Kittrell C, Ma JP, Hauge RH, Weisman RB, Smalley RE. Band gap fluorescence from individual single-walled carbon nanotubes. *Science*. 2002;297:593–596.
43. Cathcart H, Quinn S, Nicolosi V, Kelly JM, Blau WJ, Coleman JN. Spontaneous debundling of single-walled carbon nanotubes in DNA-based dispersions. *J Phys Chem C*. 2007;111:66–74.
44. Arnold MS, Green AA, Hulvat JF, Stupp SI, Hersam MC. Sorting carbon nanotubes by electronic structure using density differentiation. *Nat Nanotechnol*. 2006;1:60–65.
45. Arnold MS, Stupp SI, Hersam MC. Enrichment of single-walled carbon nanotubes by diameter in density gradients. *Nano Lett*. 2005;5: 713–718.
46. Carver RL, Peng H, Sadana AK, Nikolaev P, Arepalli S, Scott CD, Billups WE, Hauge RH, Smalley RE. A model for nucleation and growth of single wall carbon nanotubes via the HiPco process: a catalyst concentration study. *J Nanosci Nanotechnol*. 2005;5:1035–1040.
47. Shiren W, Zhiyong L, Ben W, Chuck Z. Statistical characterization of single-wall carbon nanotube length distribution. *Nanotechnology*. 2006;17:634–639.
48. Fagan JA, Landi BJ, Mandelbaum I, Simpson JR, Bajpai V, Bauer BJ, Migler K, Hight Walker AR, Raffaelle R, Hobbie EK. Comparative measures of single-wall carbon nanotube dispersion. *J Phys Chem B*. 2006;110:23801–23805.
49. Bachilo SM, Strano MS, Kittrell C, Hauge RH, Smalley RE, Weisman RB. Structure-assigned optical spectra of single-walled carbon nanotubes. *Science*. 2002;298:2361–2366.
50. Bertoncini P, Gresil M, Lardoux J, Riou I, Chauvet O. Morphology of DNA/single walled nanotubes complexes. *Dig J Nanomater Biostruct*. 2007;2:293–297.
51. Zheng M, Jagota A, Strano MS, Santos AP, Barone P, Chou SG, Diner BA, Dresselhaus MS, McLean RS, Onoa GB, Samsonidze GG, Semke ED, Usrey M, Walls DJ. Structure-based carbon nanotube sorting by sequence-dependent DNA assembly. *Science*. 2003; 302:1545–1548.
52. Niyogi S, Boukhalfa S, Chikkannanavar SB, McDonald TJ, Heben MJ, Doorn SK. Selective aggregation of single-walled carbon nanotubes via salt addition. *J Am Chem Soc*. 2007;129:1898–1899.

53. Duque JG, Densmore CG, Doorn SK. Saturation of surfactant structure at the single-walled carbon nanotube surface. *J Am Chem Soc*. 2010;132:16165–16175.
54. Duque JG, Cognet L, Parra-Vasquez ANG, Nicholas N, Schmidt HK, Pasquali M. Stable luminescence from individual carbon nanotubes in acidic, basic, and biological environments. *J Am Chem Soc*. 2008;130:2626–2633.
55. Fagan JA, Becker ML, Chun JH, Nie PT, Bauer BJ, Simpson JR, Hight-Walker A, Hobbie EK. Centrifugal length separation of carbon nanotubes. *Langmuir*. 2008;24:13880–13889.
56. Lopez F, Samseth J, Mortensen K, Rosenqvist E, Rouch J. Micro- and macrostructural studies of sodium deoxycholate micellar complexes in aqueous solutions. *Langmuir*. 1996;12:6188–6196.
57. Moore VC, Strano MS, Haroz EH, Hauge RH, Smalley RE, Schmidt J, Talmon Y. Individually suspended single-walled carbon nanotubes in various surfactants. *Nano Lett*. 2003;3:1379–1382.
58. Pagani G, Green MJ, Poulin P, Pasquali M. Competing mechanisms and scaling laws for carbon nanotube scission by ultrasonication. *Proc Natl Acad Sci USA*. 2012;109:11599–11604.
59. Lucas A, Zakri C, Maugey M, Pasquali M, van der Schoot P, Poulin P. Kinetics of nanotube and microfiber scission under sonication. *J Phys Chem C*. 2009;113:20599–20605.
60. Heller DA, Barone PW, Swanson JP, Mayrhofer RM, Strano MS. Using Raman spectroscopy to elucidate the aggregation state of single-walled carbon nanotubes. *J Phys Chem B*. 2004;108:6905–6909.
61. Fakhri N, MacKintosh FC, Lounis B, Cognet L, Pasquali M. Brownian motion of stiff filaments in a crowded environment. *Science*. 2010;330:1804–1807.

Manuscript received Sept. 27, 2013, and revision received Nov. 26, 2013.